Angle Sensitive Optical Sensor for Light Source Tracker Miniaturization

Romijn, Joost; Sanseven, Seçil; Zhang, Guoqi; Vollebregt, Sten; Sarro, Pasqualina M.

DOI
10.1109/LSENS.2022.3175607

Publication date
2022

Document Version
Final published version

Published in
IEEE Sensors Letters

Optical sensors

Angle Sensitive Optical Sensor for Light Source Tracker Miniaturization

Joost Romijn* , Seçil Şanseven, Guoqi Zhang*** , Sten Vollebregt** , and Pasqualina M. Sarro***

Laboratory of Electronic Components, Technology, and Materials (ECTM), Department of Microelectronics, Delft University of Technology, 2628 CD Delft, The Netherlands

**Member, IEEE*

***Senior Member, IEEE*

****Fellow, IEEE*

Manuscript received January 16, 2022; revised April 15, 2022; accepted May 3, 2022. Date of publication May 20, 2022; date of current version May 27, 2022.

Abstract—An angle sensitive optical sensor without conventional optics is presented in this article. The reported device omits the need for adding 3-D optics in postprocessing by monolithic integration of complimentary metal-oxide semiconductor compatible diffraction grating layers, which cuts down the fabrication costs and allows for miniaturization of these types of sensors. The sensor resolves angular information from a monochromatic light source over a single axis with a mean absolute accuracy of 0.6° in an investigated ±26° field-of-view using four unique pixels. This letter facilitates miniaturization of light source trackers, such as sun position sensors on small satellites of the future.

Index Terms—Optical sensors, angle sensitive pixels (ASPs), diffraction gratings, optical sensor, opto-electronic system, sun position sensor.

I. INTRODUCTION

Light source trackers are a sensor family that is not often seen in daily life. Still, this type of sensor is vital in aerospace applications where the movement of the spacecraft needs control. This activity is called attitude control and relies on the direction toward a known reference. Typically, this reference is the sun, and the spacecraft relies on a sun position sensor for the determination of its direction. The sun position sensor has different implementations, classified by the collimating, sun-pointing, tilted mount, and hybrid sensors [1]. The collimating sensor is adopted in most of the state-of-the-art and commercial devices. Reports of miniaturized examples include an active pixel sensor (APS) array [2] and pixel line sensor [3], which contain hundreds of individual photodetectors on a chip of few tens of mm^2.

The benefits of miniaturization in microfabrication are recognized in spacecraft design by not just adding miniaturized instruments but also scaling down the entire system. This led to the adoption of the nano satellite format, or CubeSat, which has the form factor of a carton of milk. These spacecraft still have powerful systems on board and have lower launch costs, while the bigger requirements are fulfilled by employment of a constellation of similar CubeSats. Scaling down further reduces the cost more, which opens low-cost applications in space. As such, the form factor is reduced to implement pico satellites, which are very similar to the CubeSat concept. Femto satellites, or PCBSats, are the size of a single printed circuit board (PCB) with a weight below a kilogram [4]. Even smaller are the AttoSats, or ChipSats, that are the size of a single chip with a weight of a few grams [5]. To keep up with the satellite miniaturization trend, it is vital that the sun position sensor functionality can be integrated on PCB or even chip level. This demands drastically new approaches to the implementation of the sun position sensor where the bulky collimator, which is typically fabricated by a suspended membrane or an optical window, is replaced by making the photodetectors themselves angle sensitive.

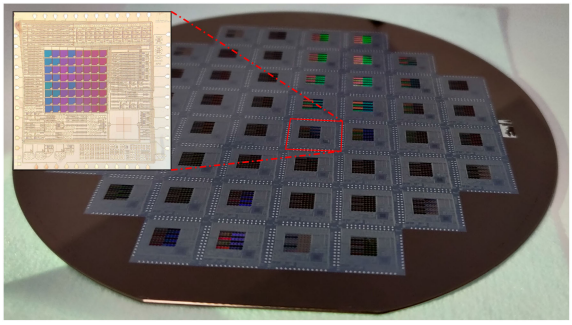

Fig. 1. Photograph of the 4-in wafer after the BICMOS7 fabrication with added module for the two-level grating layers, with the inset highlighting a microphotograph of the single 10 × 10 mm chip.

Previous work on angle sensitive pixels (ASPs) by Gill *et al.* focused on the miniaturization of focusing cameras, by implementation of planar Fourier capture arrays (PFCAs) through the use of unique diffraction gratings on each ASP. These gratings are spaced much closer to the complimentary metal-oxide semiconductor (CMOS) chip then conventional optics, thus allowing direct implementation during the wafer-level microfabrication. Besides miniaturization, the planar nature of these sensors allows for a close to ideal field-of-view of 180°. Such lensless devices fill the size gap between single photodetectors and the smallest cameras, while retaining full compatibility with conventional fabrication technologies. Each individual ASP in a PFCA is a single point in the planar Fourier space, which needs to be captured completely to transform the array output to an actual image [6], [7]. As such, careful considerations are to be made when tiling the Fourier space through design variation of each ASP [8].

This letter reports on an angle sensitive optical sensor (Fig. 1), which is the first of its kind to be used as light source tracker, that is designed

Corresponding author: Joost Romijn (e-mail: J.Romijn@tudelft.nl).

Associate Editor: Huikai Xie.

Digital Object Identifier 10.1109/LSENS.2022.3175607

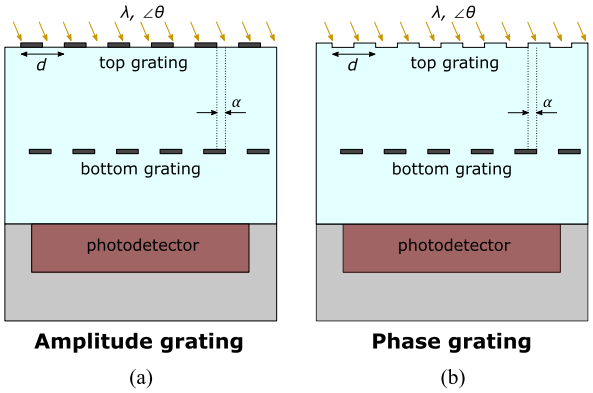

Fig. 2. Schematic illustration of (a) amplitude grating and (b) phase grating architectures that include two opaque grating layers in a transparent dielectric and a photodetector. The top and bottom gratings are also referred to as diffraction and analyzer gratings.

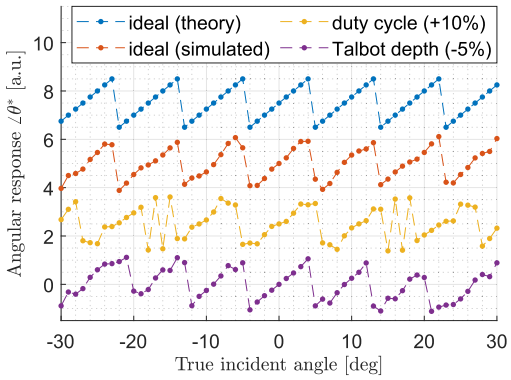

Fig. 3. Angular response $\angle\theta^*$ as a result of simulation of the ASPs considering different effects. The individual ASP simulation results are combined through (4). The curves are shifted to improve readability.

and verified for 625 nm light. The described sensor is an extension on a previously reported opto-electronic system [9], which offers 64 addressable pixels with on-chip control and readout electronics. As this sensor focuses on light source tracking rather than capturing an image, the tiling considerations of previous works on this imaging method are greatly relaxed, which results in an even smaller device of only 12 pixels instead of hundreds.

II. ANGLE SENSITIVE PIXEL DESIGN

A. Diffraction Gratings

The lensless imager exploits the Talbot effect, which is the forming of strong intensity patterns at specific distances of illuminated periodic masking layers. These patterns are referred to as self-images and occur at integer multiples of the Talbot depth, as calculated by

$$z_T = 2\frac{d^2}{\lambda} \tag{1}$$

where d is the grating pitch, and λ is the wavelength of the incident light. Note that this relation is not dependent on the incident angle of the light. To compare different ASP architectures, the unitless angular sensitivity is defined by

$$\beta = 2\pi\frac{z_T}{nd} \tag{2}$$

where n is the refractive index of the dielectric. Two main types of ASPs that make use of the Talbot effect are based on amplitude gratings or phase gratings. Amplitude gratings [see Fig. 2(a)] consist of two identical opaque layers of periodic gratings that are separated by a certain multiple of Talbot depths. Phase gratings [see Fig. 2(b)] implement the top grating layer directly in the transparent layer, which results in similar behavior but with higher quantum efficiency [10]. Placing a photodetector below the grating stack effectively integrates the generated pattern, and its output is calculated by

$$R(\angle\theta) = I_0\left(1 - m\cos\left(\beta\angle\theta + \alpha\right)\right)F(\angle\theta) \tag{3}$$

where I_0 is the intensity coefficient, m is the modulation depth, α is the phase offset, and $F(\angle\theta)$ is the nonidealities and noise in the system.

B. Readout Methodology

The response of a single ASP in (3) contains both angle and intensity information on the incident light. To obtain the angle information of the incident light, it is necessary to either know the intensity or employ a differential measurement that eliminates the need for this information. This work focuses only on amplitude gratings and uses ASPs with different phase offsets in the gratings, which allows for extraction of the angle information through

$$\angle\theta^* = \frac{1}{\beta}\tan^{-1}\left(\frac{R_{\pi/2}(\angle\theta) - R_{3\pi/2}(\angle\theta)}{R_0(\angle\theta) - R_\pi(\angle\theta)}\right) \tag{4}$$

where R_0, $R_{\pi/2}$, R_π, and $R_{3\pi/2}$ correspond to pixels with phase shifts of 0, $\pi/2$, π, and $3\pi/2$, respectively. Note that the found $\angle\theta^*$ is periodic in nature; so one has to identify the period as well to come to the actual angle. This is done through

$$\angle\theta = \angle\theta^* + pN_i \tag{5}$$

where p is the period of $\angle\theta^*$ and N_i is the amount of periods from the origin. To identify the period for fine angle detection, a course nonperiodic ASP is included. For example, a previous hybrid implementation demonstrated this concept using polarization and Talbot ASPs [11]. Typically, one needs two ASPs per axis for the course angle detection. This work does not focus on the course ASP integration; so the period of the Talbot ASPs is identified manually.

C. Simulation of the Optical Sensor

The optical response of a each individual ASP is simulated in COMSOL Multiphysics software for specific incident angles. The resulting outputs are loaded and combined in MATLAB to extract the angular response using (4), of which the resulting curves of different cases are given in Fig. 3. The simulation result of the ideal simulated ASPs show some distortion, which is caused by inescapable effects like reflection inside the grating stack.

The grating pitch inversely affects the period of the sensor response, where a larger grating pitch results in smaller sensor response period. Consequently, the angular sensitivity goes up for a larger grating pitch [see eqs. (1) and (2)]. The vertical distance affects the period and angular sensitivity of the sensor in a similar way [see (2)] and Fig. 3 shows that small deviations expected from the fabrication process have a minor effect. The effect of a nonideal grating pitch duty cycle is shown in Fig. 3 and indicates severe distortion in the 15°–20° range.

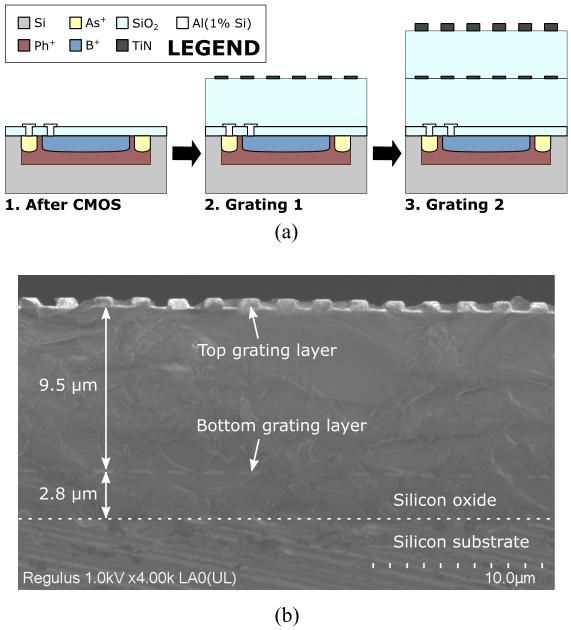

Fig. 4. Schematic illustration (a) of the diffraction grating stack fabrication steps starting after the BICMOS7 fabrication. The fabrication result (b) SEM image of the cross section of a device with 2-μm pitch in phase diffraction gratings. The oxide layer thicknesses between the substrate, first grating layer, and second grating layer are highlighted.

This demonstrates that it is crucial to optimize the fabrication of the gratings to obtain an ideal duty cycle.

The grating material reflectivity directly relates to distortion effects in the grating stack. For this reason, the gratings are implemented in TiN, which blocks the light well with a low reflectivity.

III. SAMPLE PREPARATION

A. CMOS Fabrication Technology

The CMOS opto-electronic system [9] in this work is implemented in the in-house BICMOS7 technology [12], [13], which is implemented by seven lithography masks on Si(100) 100-mm p-type wafers. The technology front end of line (FEOL) is a single well process that implements the *n*-well, and shallow *n*-type and shallow *p*-type regions. The FEOL is concluded by implementing the gate dielectric by 100-nm thermal oxide. The back end of line (BEOL) consists of two-level metal interconnect layers with corresponding via openings.

To prototype the device, the CMOS design layers are used to implement vertical photodetectors, which have a wide spectral sensitivity range [14]. These photodetectors of 0.5 × 0.5 mm are used in the three-transistor (3T) APS that implements an 8 × 8 pixel array. The pixels are electrically insulated by an implanted guard ring that implements a potential barrier to ensure that cross-talk between pixels is kept to a minimum.

B. Angle Sensitive Pixel Fabrication

The fabrication module of the double diffraction grating stack [see Fig. 4(a)] is done after completion of the BICMOS7 standard process and starts with the deposition of a 2.7-nm plasma-enhanced chemical vapor deposition (PECVD) oxide layer. This is followed by sputter deposition of the 100-nm titanium nitride (TiN) bottom grating layer, which is patterned using standard lithography and dry etching. This procedure is repeated to implement the top grating layer, using a 9.5-μm oxide and a 500-nm TiN layer. The resulting cross section of the typical stack is given in Fig. 4(b).

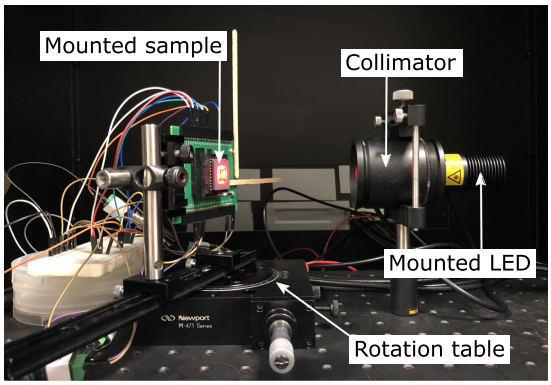

Fig. 5. Overview of the optical measurement setup which resides in a dark enclosure. The LED light source is collimated and aligned to the mounted sample, which is rotated on a table.

IV. RESULTS

A. Opto-Electrical Measurement Setup

The optical setup is depicted in Fig. 5 and consists of the 625-nm collimated light source and mounted sample that is positioned at different incident angles using a rotation table, with an estimated accuracy of 0.1°. The transient electrical measurements are performed using a microcontroller, which receives commands from a MATLAB app running on a PC. To allow interfacing between the microcontroller and the chip, analog level-shifters are used.

B. Angle Sensitive Response

The raw pixel outputs of a single sample are given in Fig. 6(a) for a fixed angle. Each readout cycle starts with the reset (RST) of the pixel to its maximum accumulated charge level. Concurrently, the generated photocurrent depletes this charge, resulting in linear decrease of the pixel output over time. The readout cycle spans a full clock (CLK) cycle and shows that the pixel output is affected by the high-to-low transition of the clock. This is likely caused by leakage current as the surrounding on-chip system updates its state in accordance to the clock. To mitigate this effect, only the first half of the clock cycle is captured during pixel readout. The technology could be improved by better electrical isolation of the individual devices, such as shallow trench isolation.

The slope is determined from the captured linear decay of each pixel, which is proportional to the generated photocurrent. The extracted slopes are used as inputs $V_i(\angle\theta)$ in (4) to find the corresponding angle $\angle\theta^*$. The results for an incident angle sweep over a single axis are given in Fig. 6(b), with good compliance to the simulation results of the same conditions. The most noticeable difference is that the slightly larger angular period predicted by simulation, which is likely due to process deviations such as the deposited oxide layers.

The periodic response of Fig. 6(b) is transformed to the full angular range response reported in Fig. 6(c). First, manual identification of the periods is performed with a fitted β for each period, resulting in a mean absolute accuracy (MAA) of 0.3° and 0.4° for the simulation and measurement results, respectively. However, such a lookup table is

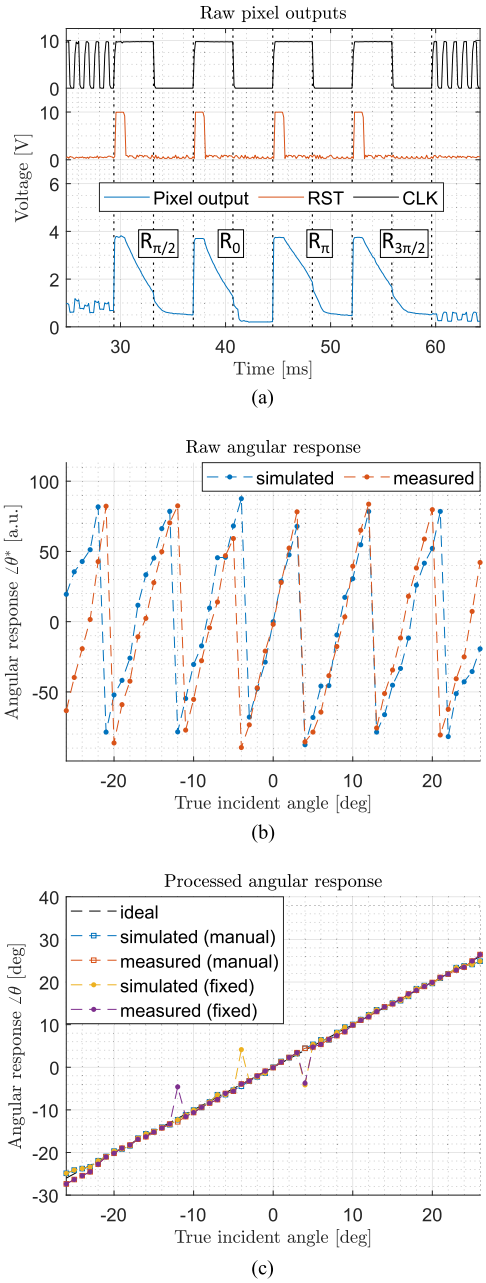

Fig. 6. Measurement results of (a) raw pixel outputs for a fixed incident angle. The fast CLK before and after the pixels of interest quickly cycles through the 64-pixel array. Derived (b) angular response using the extracted slope of each pixel [see (4)] and (c) processed response by manually identified or fixed angular periods [see (5)].

not desirable for device operation and so a fixed period and β are used by taking the means of the list from manual identification, resulting in an increased MAA of 0.6° for both simulation and measurement. Note that in the fixed case, several offsets occur at the edges of angular periods, which is due to a combination of offsets in the measurement setup and nonidealities in the device.

At this stage, the angle sensitive optical sensor is not yet verified for different wavelengths or broadband light, but the signal is expected to be severely distorted by contributions of other wavelengths for which the architecture is not optimized. Therefore, future work regarding broad-spectrum illumination would benefit from integration of optical bandpass filters or odd-symmetry spiral phase gratings [15].

V. CONCLUSION

The reported four pixel fine ASP image sensor is able to resolve angular information over a single axis with a MAA of 0.6° in the investigated ±26° field-of-view. The sensor was fabricated by monolithic integration of a double grating stack on top of a CMOS active pixel platform. Angular period identification is done in postprocessing and requires integration of course ASPs to perform this on-chip. Together with the addition of perpendicular fine ASPs for angular detection on two axis, 12 pixels are required.

Future work benefits from implementation in phase grating ASPs, to increase the quantum efficiency, and additional grating pitches, to improve the accuracy at the limits of each angular period. Finally, the next generation should consider broadband light sources, toward application as a miniaturized sun position sensor.

ACKNOWLEDGMENT

The authors would like to thank the Delft University of Technology Else Kooi Laboratory staff for processing support. Furthermore, the authors would like to thank the Applied and Engineering Sciences (AES) which is part of The Netherlands Organization for Scientific Research (NWO), and which is partly funded by the Ministry of Economic Affairs, for financially supporting this work under Project 16247.

REFERENCES

[1] L. Salgado-Conrado, "A review on sun position sensors used in solar applications," *Renewable Sustain. Energy Rev.*, vol. 82, pp. 2128–2146, 2018.

[2] N. Xie and A. J. P. Theuwissen, "Low-power high-accuracy micro-digital sun sensor by means of a CMOS image sensor," *J. Electron. Imag.*, vol. 22, no. 3, 2013, Art. no. 0 33030.

[3] Ł. Farian, P. Häfliger, and J. A. Leñero-Bardallo, "A miniaturized two-axis ultra low latency and low-power sun sensor for attitude determination of micro space probes," *IEEE Trans. Circuits Syst. I: Regular Papers*, vol. 65, no. 5, pp. 1543–1554, May 2018.

[4] D. J. Barnhart *et al.*, "A low-cost femtosatellite to enable distributed space missions," *Acta Astronautica*, vol. 64, pp. 11–12, 2009.

[5] A. M. Hein, Z. Burkhardt, and T. M. Eubanks, "Attosats: Chipsats, other gram-scale spacecraft, and beyond," *Instrum. Methods Astrophys.*, 2019, *arXiv:1910.12559*.

[6] P. R. Gill *et al.*, "Robustness of planar fourier capture arrays to colour changes and lost pixels," in *J. Instrum.*, vol. 7, 2012, Art. no. C01061.

[7] P. R. Gill *et al.*, "A microscale camera using direct fourier-domain scene capture," *Opt. Lett.*, vol. 36, pp. 2949–2951, 2011.

[8] P. R. Gill and A. Molnar, "Scaling properties of well-tiled PFCAs,," in *Imaging and Applied Optics Technical Papers*. Washington, DC, USA: Optica Publishing Group, 2012, Paper j W3A.3.

[9] J. Romijn *et al.*, "Towards a scalable sun position sensor with monolithic integration of the 3D optics for miniaturized satellite attitude control," in *Proc. IEEE 34th Int. Conf. Micro Electro Mech. Syst.*, 2021, pp. 642–645.

[10] S. Sivaramakrishnan *et al.*, "Enhanced angle sensitive pixels for light field imaging," in *Proc. Int. Electron Devices Meeting*, 2011, pp. 8.6.1–8.6.4.

[11] V. Varghese and S. Chen, "Polarization-based angle sensitive pixels for light field image sensors with high spatio-angular resolution," *IEEE Sensors J.*, vol. 16, no. 13, pp. 5183–5194, Jul. 2016.

[12] H. W. van Zeijl and L. K. Nanver, "A low-cost BiCMOS process with metal gates," in *Proc. Mater. Res. Soc. Symp.*, vol. 611, 2001, Art. no. 721 .

[13] Z. Kolahdouz *et al.*, "Silicon-based multi-functional wafer-level-package for LEDs in a 7-mask BiCMOS process," *Sens. Actuators A: Phys.*, vol. 263, pp. 622–632, 2017.

[14] Z. Kolahdouz *et al.*, "Output blue light evaluation for phosphor based smart white LED wafer level packages," *Opt. Exp.*, vol. 24, no. 4, pp. 3216–3229, 2016.

[15] P. R. Gill and D. G. Stork, "Lensless ultra-miniature imagers using odd-symmetry spiral phase gratings," in *Imaging and Applied Optics Technical Papers*. Washington, DC, USA: Optica Publishing Group, 2013, Paper c W4C.3.